



1 **Highly accurate dating of micrometre-scale baddeleyite domains through combined**
2 **focused ion beam extraction and U-Pb thermal ionisation mass spectrometry (FIB-TIMS)**

3 Lee F White^{1,2*}, Kimberly T Tait^{1,2}, Sandra L Kamo^{1,3}, Desmond E Moser⁴ & James R Darling⁵

4 ¹Department of Natural History, Royal Ontario Museum, Toronto, Ontario, M5S 2C6, Canada

5 ²Department of Earth Sciences, University of Toronto, Toronto, Ontario, M5S 3B1, Canada

6 ³Jack Satterly Lab, University of Toronto, Toronto, Ontario, M5S 3B1, Canada

7 ⁴Western University, London, Ontario, Canada

8 ⁵School of the Environment, Geography and Geosciences, University of Portsmouth, PO1 3QL, UK

9 *Corresponding Author; lwhite@rom.on.ca

10

11 **Baddeleyite is a powerful chronometer of mafic magmatic and meteorite impact**
12 **processes. High precision and accuracy U-Pb ages can be measured from single grains by**
13 **isotope dilution thermal ionisation mass spectrometry (ID-TIMS), but this requires**
14 **destruction of the host rock for highly challenging grain isolation and dissolution. As a**
15 **result, the technique is rarely applied to precious samples with very limited availability**
16 **(such as lunar, Martian and asteroidal meteorites and returned samples) or samples**
17 **containing small baddeleyite grains that cannot readily be isolated by conventional**
18 **mineral separation techniques. Here, we use focused ion beam (FIB) techniques, utilising**
19 **both Xe⁺ plasma and Ga⁺ ion sources, to liberate baddeleyite subdomains *in situ*, allowing**
20 **their extraction for ID-TIMS dating. We have analysed the U-Pb isotope systematics of**
21 **domains ranging between 200 µm and 10 µm in length and 5 µg to 0.1 µg in mass. In total,**
22 **seven domains of Phalaborwa baddeleyite extracted using a Xe⁺-pFIB yield a weighted**
23 **mean ²⁰⁷Pb/²⁰⁶Pb age of 2060.1 ± 2.4 Ma (0.12 %; all uncertainties 2σ), within uncertainty**
24 **of reference values. The smallest extracted domain (ca. 10x15x10 µm) yields an internal**
25 **²⁰⁷Pb/²⁰⁶Pb uncertainty of ± 0.15 %. Comparable levels of precision are achieved using a**
26 **Ga⁺-source FIB instrument (± 0.20 %), though the slower cutting speed limits potential**
27 **application to larger grains. While the U-Pb data are between 0.5 and 13.6 % discordant,**
28 **the results generate a precise upper intercept age in U-Pb concordia space of 2061.1 ± 7.4**
29 **Ma (0.72%). Importantly, the extent of discordance does not correlate with the ratio of**
30 **material to ion-milled surface area, showing that FIB extraction does not induce**
31 **disturbance of U-Pb systematics in even the smallest extracted domains. Instead, we**
32 **confirm the natural U-Pb variation and discordance within the Phalaborwa baddeleyite**
33 **population observed with other geochronological techniques. Our results demonstrate the**



34 **FIB-TIMS technique to be a powerful tool for high-accuracy *in-situ* U-Pb dating, allowing**
35 **dating of a wide variety of targets and processes newly accessible to geochronology.**

36 *Keywords: FIB-TIMS; FIB; TIMS; U-Pb; Baddeleyite; Geochronology; In-situ*

37

38 **1.0 Introduction**

39 The generation of high precision chronological data is a cornerstone of the Earth and planetary
40 sciences, providing an absolute measurement on which to anchor relative observations of
41 geological time (e.g. Gradstein et al., 2004). The most precise radiogenic isotopic ratios (e.g.
42 U-Th-Pb, Sm-Nd, Rb-Sr) are generated using isotope dilution thermal ionisation mass
43 spectrometry (ID-TIMS; Parrish and Noble, 2003), which has been used to measure the timing
44 of Solar System formation (Amelin et al., 2002), initial differentiation of the Moon (Barboni
45 et al., 2017), and the timing of crustal formation on Mars (Bouvier et al., 2018), often with
46 internal age uncertainties on the order of $\sim 0.1\%$ 2σ . In particular, U-Pb isotopic measurements
47 of the accessory minerals zircon ($ZrSiO_4$) and baddeleyite (ZrO_2) by ID-TIMS allows for
48 direct, high precision dating of magmatic, metamorphic, and shock metamorphic events (e.g.
49 Parrish and Noble., 2002; Bouvier et al., 2018).

50

51 To attain the improved precision and accuracy offered by ID-TIMS mineral grains have to be
52 disaggregated from their host rock using crushing and sieving techniques or electric pulse
53 disaggregation before separation based on the density, magnetic and optical properties of the
54 target mineral phase (e.g. Söderlund and Johansson, 2002). As a result, the analysed grains
55 preserve no evidence for their petrological or mineralogical context and cannot be characterised
56 (e.g. electron microscopy) prior to dating, which makes the accurate interpretation of U-Th-Pb
57 ages in samples with complex thermal, metamorphic and deformation histories highly
58 challenging (e.g. Bouvier et al., 2018). In addition, the small grain size (commonly $< 50 \mu m$)
59 and bladed nature of individual baddeleyite crystals makes clean separation of target grains
60 incredibly time consuming (e.g. Söderlund and Johansson, 2002). Though grains can be
61 chemically or physically abraded to remove potentially discordant crystallographic domains
62 (Krogh, 1982), ID-TIMS is incapable of separating crystallographic domains of potentially
63 different ages, such as micrometre-scale recrystallized or altered domains in shocked minerals
64 which may record disturbed U-Pb isotope reservoirs (Cavosie et al., 2015; White et al.,
65 2017a,b). These realities mean that, although ID-TIMS delivers the highest accuracy and
66 precision isotopic data, it has historically remained challenging to impossible to apply to rare
67 meteoritic or returned planetary materials, or mineral targets located within thin sections.



68 Developing the capability to extract accessory phases directly from a thin section or subsample
69 target domains within grain mount would be incredibly powerful, allowing for the generation
70 of relatively high precision radiogenic ages from microstructurally and chemically
71 characterised grains (Moser et al., 2011, 2013; Darling et al., 2016) which retain petrological
72 and mineralogical evidence for their crystallization or metamorphism; information critical to
73 accurately interpreting isotopic ages.

74

75 Focused ion beam (FIB) technologies are a staple of the material sciences, most commonly
76 used to fabricate and analyse nanomaterials (Matsui et al., 2000; Schaffer et al., 2012). Within
77 the Earth and planetary sciences, FIB's have principally been used to prepare thin foils for
78 analysis of materials by transmission electron microscopy (TEM), which requires a sample to
79 be electron transparent (Heaney et al., 2001), and the preparation of microtip specimen for
80 atom probe tomography (e.g. Reddy et al., 2016). Although Ga⁺ source FIB's are the most
81 common, the linear relationship between beam current and spot size prevents operation of the
82 instrument at high currents (> 20 nA), limiting the rate (and thus volume) of material removal
83 to the tens of micrometres in a single day session. Options for the removal of larger masses
84 require higher energy; for example, laser cutting allows extraction of millimetre-scale sections
85 of material but induces deeper and more severe damage to the milled surface (Echlin et al.,
86 2012), and in the case of geological materials may result in localised fractionation of target
87 elements and isotopes comparable to LA-ICP-MS (e.g. Ibanez-Mejia et al., 2014). Such side
88 effects are not induced by micro-drill extraction of target phases (e.g. Paquette et al., 2004),
89 but the spatial resolution offered by such an approach is incapable of isolating exceptionally
90 small (< 50 µm) domains, such as meteoritic micro-baddeleyite (Herd et al., 2018).

91

92 Recent advances in FIB technologies have significantly broadened the range of ion beam
93 chemistries and source types, the most recent of being the magnetically enhanced, inductively
94 coupled Xenon (Xe⁺) plasma ion source (Bassim et al., 2014). While a Ga⁺ liquid metal ion
95 source (LMIS) FIB loses special resolution at higher currents (I) due to spherical aberration
96 resulting in a non-Gaussian beam shape with large tails (Smith et al., 2006; Bassim et al., 2014),
97 the Xe⁺ ICP source remains stable beyond ~60 nA. As a result, a finer spot size can be achieved
98 for the same focussing optics using a Xe⁺ pFIB, while the superior angular intensity allows for
99 high current milling as the effects of spherical aberration are not realised (Smith et al., 2006).
100 This makes the attainment of currents in the µA range possible with a Xe⁺ pFIB, which cannot
101 be achieved with a Ga⁺ LMIS instrument whilst retaining a focused beam (Figure 1). Another



102 important benefit of the Xe⁺ pFIB is a direct result of the larger ionic size of Xe⁺ compared to
103 Ga⁺ (e.g. Yuan et al., 2017), which results in more atoms of material being ejected from the
104 target per incident ion and yielding a higher removal rate. Though sputtering rates are typically
105 on the order of 10 - 30% higher for Xe⁺ compared to Ga⁺, Cu (~300% higher) and Si (30 - 50%
106 higher) demonstrate notably higher sputter rates per coulomb when exposed to a Xe⁺ ion beam
107 (Ziegler et al., 1985). The larger ionic size of Xe⁺ also results in a shallower depth of ion
108 penetration and resulting damage to the target material; for example, the penetration of Ga⁺
109 and Xe⁺ in Si is 24 nm and 28 nm respectively at 30 kV (Ziegler et al., 1985; Burnett et al.,
110 2016). However, the effect of this interaction, which often results in amorphisation of the
111 surface layer exposed to the ion beam, on trace element distribution and mobility is poorly
112 constrained. For example, the effect on U and Pb mobility is unknown. In this study, we analyse
113 multiple samples of the Phalaborwa U-Pb baddeleyite reference material, which have been
114 extracted *in-situ* via Ga⁺ FIB, Xe⁺ pFIB, and by mechanical (non-FIB) fragmentation to test
115 for structural damage, heating and ion implantation during FIB exposure, establishing a new
116 approach to high precision ID-TIMS analysis and demonstrating the potential for Xe⁺ FIB
117 techniques to extract grains from thin section.

118

119 **2.0 Sample and methodology**

120 Originally sampled from the Phalaborwa complex (a composite intrusion of cumulate
121 clinopyroxenites related to pulsed carbonatite magma emplacement) in South Africa,
122 baddeleyite grains from the locality are often used as a reference material in U-Th-Pb studies
123 (Reischmann, 1995; Heaman, 2009; Schmitt et al., 2010). A single large crystal of Phalaborwa
124 baddeleyite was acquired from the same sample at the Royal Ontario Museum as studied by
125 (Heaman, 2009), who undertook 68 ID-TIMS measurements of 2 to 384 mg fragments of this
126 material. These fragments are variable in U concentration (51 - 2124 ppm) and the majority of
127 U-Pb analyses from Heaman (2009) are < 1 % discordant (58/68), although individual analyses
128 are up to 10 % discordant (taken as ²⁰⁷Pb/²⁰⁶Pb age over ²⁰⁶Pb/²³⁸U age). A precise weighted
129 mean ²⁰⁷Pb/²⁰⁶Pb age of 2059.60 ± 0.35 Ma from that study is taken as the best measure of the
130 crystallization age. Variations in U content and U-Pb age have also been reported during higher
131 spatial resolution isotopic analyses of Phalaborwa, such as depth profiling laser ablation
132 inductively coupled plasma mass spectrometry (LA-ICP-MS) (Ibanez-Mejia et al., 2014).
133 During 326 small volume LA-ICP-MS analyses of Phalaborwa baddeleyite, U concentration
134 (87 - 1478 ppm) and percentage discordance (< 13.7 %) vary substantially, while the majority



135 (77%) of U-Pb analyses are >1 % discordant (Ibanez-Mejia et al., 2014). Notably, 30 of these
136 analyses are highly discordant (> 5 % discordance).

137

138 ***2.1 Focused ion beam (FIB) extraction of target domains***

139 A large (~5 cm) grain of Phalaborwa baddeleyite was taken from the mineralogy collection at
140 the Royal Ontario Museum, Toronto, Canada, for use in this study (accession number
141 M37144). The grain was mounted in epoxy and polished to expose the surface of the grain
142 using 6 µm, 1 µm and 0.5 µm grit diamond paste. The epoxy mount was secured to an SEM
143 stub and coated with a 15 nm thick carbon coat prior to imaging and FIB work. A Thermo
144 Scientific Helios G4 UXe DualBeam pFIB at the Canadian Centre for Electron Microscopy
145 (CCEM) in McMaster University, Canada, and a Hitachi NB5000 Ga-FIB at the Ontario Centre
146 for the Characterisation of Advanced Materials (OCCAM) in the University of Toronto,
147 Canada, were used in this study.

148

149 The Xe-pFIB was operated at 30 kV, 2.5 µA for the largest cuts, facilitating the extraction of a
150 100x100x100 µm cube domain of baddeleyite in 32 minutes and two 200x50x30 µm
151 rectangular domains in 21 minutes each. Two small (5x15x10 µm) cuboids of baddeleyite were
152 completely isolated by 2 minutes of Xe-pFIB exposure. The Ga-FIB was operated at 40 kV
153 and >50 nA (estimated current from previous calibration), taking two hours to isolate a
154 50x50x50 µm cube domain. In all scenarios a small amount of material (<5 µm wide) was left
155 to anchor the isolated domain to the host mount (Figure 2). This allowed transportation of the
156 grain mount to the Jack Satterly lab for extraction without the use of platinum or tungsten weld,
157 which may contain unconstrained levels of common Pb. The grain mount was placed in a large
158 petri dish before being entirely submerged in ethanol. Fine tipped tweezers and custom pipettes
159 (made within the Jack Satterly Lab) were used to physically knock the FIB'ed material loose
160 under an optical microscope, where it became suspended in the alcohol layer before being
161 transferred to a separate dish for drying and imaging. Following extraction, the tip of one of
162 the 200x50x30 µm rectangles was physically broken to produce two smaller (< 15 µm)
163 domains consisting of outer surface areas which have been both FIB'ed and not FIB'ed. These
164 FIB'ed domains were augmented by gouging six chips (200 µm to 3 mm in size) of material
165 from the same mounted grain to test the larger-scale homogeneity of the target material, which
166 were separated into two aliquots, and two smaller grains separated and supplied as an existing
167 U-Th-Pb reference material were also analysed. In total, twelve TIMS analysis are incorporated



168 into this study; two whole ($< 40 \mu\text{m}$) baddeleyite grains, and ten subsampled domains of the
169 large mounted grain; two aliquots of material physically carved out with no FIB exposure, one
170 subdomain with Ga-FIB extraction, and seven using Xe-pFIB extraction.

171

172 **2.2 U-Pb thermal ionisation mass spectrometry (TIMS)**

173 U–Pb geochronology was conducted at the Jack Satterly Geochronology Laboratory,
174 Department of Earth Sciences, at the University of Toronto. Grain weights were estimated from
175 photomicrographs, aided by known size dimensions of grains from FIB preparation. The grains
176 were washed in 8N HNO_3 before being loaded into dissolution vessels with a mixed ^{205}Pb –
177 ^{235}U isotopic tracer solution. Baddeleyite was dissolved using ~ 0.10 ml of concentrated
178 hydrofluoric acid (HF) and ~ 0.02 ml of 8N nitric acid (HNO_3) at 200°C (Krogh, 1973) for up
179 to 5 days, then dried to a precipitate, and re-dissolved in ~ 0.15 ml of 3N hydrochloric acid
180 (HCl). Uranium and lead were isolated from the solutions using anion exchange
181 chromatography, dried in dilute phosphoric acid (H_3PO_4), and deposited onto outgassed
182 rhenium filaments with silica gel (Gerstenberger and Haase, 1997). U and Pb were analysed
183 with a VG M354 mass spectrometer in dynamic mode with a Daly pulse-counting system. The
184 dead time of the Daly measuring system for Pb and U was 16.5 and 14.5 ns, respectively. The
185 mass discrimination correction for the Daly detector is constant at 0.05 %/atomic mass unit.
186 Daly characteristics were monitored using the SRM 982 Pb standard. Thermal mass
187 fractionation was measured and corrected within each cycle for both Pb and U. Given the
188 pristine nature of the FIB-extracted baddeleyite domains, the total common Pb in each
189 baddeleyite analysis was attributed to laboratory Pb (corrected using an isotopic composition
190 of $^{206}\text{Pb}/^{204}\text{Pb}$ of 18.49 ± 0.4 %, $^{207}\text{Pb}/^{204}\text{Pb}$ of 15.59 ± 0.4 %, $^{208}\text{Pb}/^{204}\text{Pb}$ of 39.36 ± 0.4 %; 2s
191 uncertainties), thus no correction for initial common Pb from geological sources was made.
192 Routine testing indicates that laboratory blanks for Pb and U are usually less than 0.5 and 0.01
193 pg, respectively, but common Pb can be introduced during analysis. Corrections to the
194 $^{206}\text{Pb}/^{238}\text{U}$ and $^{207}\text{Pb}/^{206}\text{Pb}$ ages for initial ^{230}Th disequilibrium have been made assuming a
195 Th/U ratio in the magma of 4.2, based on assumed crustal average values. Decay constants are
196 those of (Jaffey et al., 1971) (^{238}U and ^{235}U are 1.55125×10^{-10} and 9.8485×10^{-10} per year,
197 respectively). All age errors quoted in the text and tables, and error ellipses in the concordia
198 diagram is given at 2σ .

199



200 **3.0 Results**

201 In total, twelve TIMS analysis were conducted on grains and subdomains of the Phalaborwa
202 baddeleyite, with one sample extracted by Ga⁺ FIB, seven using the Xe⁺ pFIB, two with no
203 exposure to the FIB instruments and two entirely separate whole grains. A summary of the
204 collected U-Pb data can be seen in Table 1. Total U concentrations vary between 106 and 3027
205 ppm, in agreement with published values for Phalaborwa baddeleyite (Heaman, 2009) though
206 suggestive of highly variable uranium concentrations within individual grains of the
207 Phalaborwa baddeleyite (Ibanez-Mejia et al., 2014; Reinhard et al., 2018).

208

209 Two separate ~30 μm crystals, independent of the large grain embedded for FIB work, yield
210 concordant U-Pb ages and Pb-Pb ages with uncertainties on the order of ± 0.07% 2s. Two
211 larger (~100 μm) domains physically broken out of the baddeleyite mounted in epoxy yield
212 equally precise Pb-Pb ages of ~2062 Ma (± 0.09 % 2σ), though display < 8.4 % discordance
213 in the measured U-Pb systematics (with a youngest ²⁰⁶Pb/²³⁸U age of 1912 Ma).

214

215 All domains extracted by FIB (both Ga⁺ and Xe⁺ source) yield high precision ²⁰⁷Pb / ²⁰⁶Pb ages
216 (< 0.4 % 2σ) that are in agreement with published TIMS and SS-LA-ICPMS values (Heaman,
217 2009; Ibanez-Mejia et al., 2014). This includes 5 x 15 μm domains containing as little as ~4.5
218 pg of Pb. However, all data points, aside from the two smallest flakes broken from a 200x50x50
219 μm cuboid, are discordant (Figure 3). The most discordant analysis (13.6% discordant,
220 ²⁰⁶Pb/²³⁸U age of 1811 Ma) was generated by the smallest (5x15 μm) domain isolated by Xe-
221 pFIB, though there is otherwise no correlation between surface area exposed to the FIB and
222 severity of discordance. This is supported by the observed age overlap between the 50 μm³
223 cube prepared by Ga⁺ FIB and 100 μm³ cube prepared by Xe⁺ pFIB, which yield U-Pb ages
224 with 5.1 and 6.2% discordance, respectively. Plotting all of the TIMS data (n = 12) on a
225 concordia diagram yield a discordant array with an upper intercept of 2061.5 ± 2.8 Ma (2s),
226 while all Ga⁺ and Xe⁺ FIB-TIMS data points (n = 8) yield an upper intercept of 2061.1 ± 7.4
227 Ma.

228

229 **4.0 Discussion**

230 **4.1 FIB extraction for U-Pb isotopic analysis**

231 The effects of both the Ga⁺ and Xe⁺ FIB instruments on the U-Pb isotope systematics in
232 accessory phase geochronometers has never been explored, and thus the potential for the ion



233 beam to induce Pb diffusion and loss in exposed surface areas must be addressed for the FIB-
234 TIMS technique. While our new FIB-TIMS data are up to 13.6 % discordant, there is no
235 obvious correlation between the severity of discordance and the method used to isolate the
236 domain for TIMS dating. For example, domains physically broken away from the mount (e.g.
237 with no exposure to either the Xe⁺ or Ga⁺ FIB beam) yield U-Pb ages of 2051 ± 4 Ma and 1912
238 ± 3.4 Ma, representing the oldest and second youngest measured age of the large Phalaborwa
239 crystal incorporated into this study. The lack of correlation between measured discordance,
240 FIB ion source (Ga⁺ or Xe⁺), FIB exposure time, and subsampled domain size provides strong
241 evidence that the extracted domains represent natural heterogeneity of the large Phalaborwa
242 crystal, and not localised FIB-induced mobilisation and loss of Pb or other effects related to
243 implantation of the primary ion beam. This observation supports previous studies into FIB
244 induced damage in materials, which despite inducing up to 22 nm of surface amorphisation has
245 never been reported to induce local isotopic or elemental fractionation in the target material
246 (Schaffer et al., 2012; Burnett et al., 2016). Furthermore, the FIB-TIMS method had not led to
247 significantly higher procedural Pb blanks compared to standard chemistry, further supporting
248 the ability of FIB instruments to produce TIMS samples free of contamination and localised
249 fractionation.

250

251 ***4.2 Isotopic heterogeneity in Phalaborwa baddeleyite***

252 Single shot laser ablation (SS-LA-ICP-MS) work on Phalaborwa has revealed discrepancy
253 from measured TIMS Pb-Pb ages of between 0.1 and 2.6 %, and discordance in U-Pb
254 systematics of up to 13.7 % (Ibanez-Mejia et al., 2014). Sub micrometre scale variations in the
255 ²⁰⁶Pb/²³⁸U ratio have also been reported by atom probe analyses of Phalaborwa baddeleyite
256 (White et al., 2017b; Reinhard et al., 2018). ²⁰⁶Pb/²³⁸U ages generated by SS-LA-ICP-MS
257 (Ibanez-Mejia et al., 2014) hint at variations in age of the Phalaborwa baddeleyite reference
258 material, though the low precision of these data points (< 8.6% 2σ) may partially mask local
259 heterogeneities. By subsampling a single large grain of Phalaborwa baddeleyite, we reveal that
260 measured U-Pb ages vary by up to 227 Ma, and Pb-Pb ages vary by less than 6 Ma. It is likely
261 that the small volumes analysed by FIB-TIMS (and SIMS; c. 10 x 10 x 1 μm) act to subsample
262 natural U zonation and variation within the Phalaborwa baddeleyite standard that are otherwise
263 homogenised during larger volume analyses (e.g. whole grain TIMS or LA-ICP-MS). Care
264 must be taken going forward when using the Phalaborwa baddeleyite as a small-volume U-Pb
265 mineral standard, particularly for techniques such as FIB-TIMS or atom probe tomography
266 (Reinhard et al., 2018).



267

268 **4.3 Minimum sample sizes accessible by FIB-TIMS**

269 With the development of the Xe⁺ pFIB, the FIB-TIMS technique can be applied to *in-situ* target
270 mineral grains up to millimetres in size (e.g. Burnett et al., 2016). It is also possible to isolate
271 domains as small as ~5 μm, though manipulating such small regions under optical microscope
272 (e.g. for acid dissolution prior to ID-TIMS) is incredibly challenging and can result in the loss
273 of extracted grains. At the smallest grain sizes, ejection of daughter Pb atoms from crystal
274 surfaces through direct alpha recoil ejection can result in discordant U-Pb ages from the
275 outermost 24 nm (± 7 nm) of the baddeleyite crystal (Davis and Davis, 2017). This would only
276 become an issue when sampling small grains (< 15 μm thick) in their entirety, as the large
277 surface-area to volume ratio would potentially lead to slightly discordant U-Pb ages following
278 extensive ejection of daughter isotopes (Romer, 2003), requiring a simple linear correction on
279 the order of 0.1 - 0.5% (Davis and Davis, 2017). Subsampling internal domains of larger grains
280 will circumvent this issue, allowing the targeted extraction of centralised regions which are
281 unlikely to have lost Pb during an alpha recoil event.

282

283 An additional possible source of discordance in baddeleyite U-Pb TIMS analysis is the
284 incorporation of zircon overgrowths (which are subjected to Pb loss; Pietrzak-Renaud and
285 Davis, 2014) or surrounding common-Pb bearing phases in the extracted volume. This is not
286 an issue in FIB-TIMS as such features can be removed using the FIB instrument prior to U-Pb
287 analysis (Figure 4). While such work will significantly improve the concordance of generated
288 U-Pb ages, it will also reduce the volume of material than can be analysed by TIMS, potentially
289 increasing the risk of grain loss during extraction and manipulation.

290

291 At the smallest sample sizes, uncertainties will naturally start to increase due to the reduced
292 atoms / counts of U and Pb. However, we demonstrate that even in the smallest baddeleyite
293 domains analysed here (0.00005 mg; ~10 μm length) uncertainties on the corrected ²⁰⁶Pb/²³⁸U
294 ages do not rise above ± 0.85% 2σ. Associated Pb/Pb ages display ± 0.38 % 2σ, although a
295 ‘dirty’ run with excess common Pb yields uncertainties on the order of 2.13 % 2σ. The FIB-
296 TIMS technique also acts to circumvent any variability in measured U-Pb ratios (< 5%) induced
297 by orientation-dependent Pb/U fractionation during secondary-ion mass spectrometry
298 (Wingate and Compston, 2000; Schmitt et al., 2010) as the high energy of the FIB instrument
299 (~2.5 μA) would not induce preferential channelling of ions along low-index crystal lattice



300 orientations, comparable to laser ablation inductively coupled plasma mass spectrometry
301 analysis (Ibanez-Mejia et al., 2014).

302

303 **5.0 Conclusions**

304 We have shown that volumes as small as $\sim 5 \times 15 \mu\text{m}$ can be effectively isolated, extracted and
305 dated *in-situ* using the FIB-TIMS technique developed for this study. From these tiny domains,
306 accurate and high precision U-Pb concordia ages ($2061.1 \pm 2.6 \text{ Ma } 2\sigma$) and weighted average
307 Pb-Pb ages ($2060 \pm 1.9 \text{ Ma } 2\sigma$) can be generated. Both Ga^+ and Xe^+ source focused ion beams
308 were employed, and, while neither technique induces isotopic fractionation within the target
309 material, we recommend using a Xe^+ pFIB where possible due to the order-of-magnitude faster
310 mill rates, particularly if applying this technique to larger ($> 50 \mu\text{m}$) mineral grains and
311 subdomains. Using the FIB-TIMS technique, it is now possible to produce high precision ages
312 from mineral grains that have been extensively imaged and characterised within a thin section,
313 though extra care must be taken during the physical extraction of the smallest domains. This
314 technique will be of particular importance for meteoritic and returned samples, which are too
315 valuable to be exposed to the destructive protocol typically required for TIMS analysis and will
316 allow the generation of high precision age data from accessory phases previously inaccessible
317 to geochronology.

318

319 **Author Contributions**

320 L.F.W and J.R.D designed the study. L.F.W and S. K conducted the experiments. K.T.T and
321 D.E.M provided materials. All authors interpreted the data. L.F.W drafted the manuscript with
322 input from all co-authors.

323

324 **Acknowledgments**

325 L.F.W is supported by a Hatch Ltd. Postdoctoral fellowship. D.E.M and K.T.T are supported
326 by an NSERC discovery grant. This study was supported by an STFC grant to JRD
327 (ST/S000291/1). We thank Ian Nicklin, Tanya Kizovski, Ana Cernok (ROM), Brian Langelier
328 (McMaster University) and Gabriel Acuri (Western University) for useful discussions on
329 technique development and implementation. We thank Sal Boccia, Jane Howe (University of
330 Toronto) and Travis Casagrande (McMaster University) for assistance with and access to the
331 Ga^+ and Xe^+ focused ion beam instruments incorporated into the study.

332



333 **References**

- 334 Amelin, Y., Krot, A.N., Hutcheon, I.D., and Ulyanov, A.A.: Lead isotopic ages of chondrules
335 and calcium-aluminium-rich inclusions, *Science*, 80, 297, 1678–1683, 2002.
- 336 Barboni, M., Boehnke, P., Keller, B., Kohl, I E., Schoene, B., Young, E. D., and McKeegan,
337 K. D.: Early formation of the Moon 4.51 billion years ago, *Sci Adv*, 3:e1602365, 2017.
- 338 Bassim, N., Scott, K., and Giannuzzi, L. A.: Recent advances in focused ion beam technology
339 and applications, *MRS Bull* 39:317–325, 2014.
- 340 Bouvier, L. C., Costa, M. M., Connelly, J. N., Jensen, N. K., Wielandt, D., Storey, M.,
341 Nemchin, A. A., Whitehouse, M. J., Snape, J. F., Bellucci, J. J., Moynier, F., Agranier,
342 A., Gueguen, B., Schonbachler, M., and Bizzarro, M.: Evidence for extremely rapid
343 magma ocean crystallization and crust formation on Mars, *Nature* 558:6–11. doi:
344 10.1038/s41586018-0222-z, 2018.
- 345 Burnett, T. L., Kelley, R., Winiarski, B., Contreras, L., Daly, M., Gholinia, A., Burke, and M.
346 G., Withers, P. J.: Large volume serial section tomography by Xe Plasma FIB dual beam
347 microscopy, *Ultramicroscopy*, 161:119–129, doi:10.1016/j.ultramic.2015.11.001, 2016.
- 348 Cavosie, A. J., Erickson, T. M., Timms NE, Reddy, S. M., Talavera, C., Montalvo, S. D.,
349 Pincus, M. R., Gibbon, R. J., and Moser, D.: A terrestrial perspective on using ex situ
350 shocked zircons to date lunar impacts, *Geology*, 43:999–1002, doi: 10.1130/G37059.1,
351 2015.
- 352 Darling, J. R., Moser, D. E., Barker, I. R., Tait, K. T., Chamberlain, K. R., Schmitt, A. K., and
353 Hyde, B. C.: Variable microstructural response of baddeleyite to shock metamorphism in
354 young basaltic shergottite NWA 5298 and improved U–Pb dating of Solar System events,
355 *Earth Planet Sci Lett*, 444:1–12, doi: 10.1016/j.epsl.2016.03.032, 2016 .
- 356 Davis, W. J., and Davis, D. W.: Alpha Recoil Loss of Pb from Baddeleyite Evaluated by High
357 Resolution Ion Microprobe (SHRIMP II) Depth Profiling and Numerical Modelling:
358 Implications for the Interpretation of U–Pb Ages in Small Baddeleyite Crystals. In:
359 *Microstructural Geochronology: Planetary Records Down to Atom Scale*, 247–259, 2017.
- 360 Echlin, M., Mottura, A., Torbet, C., and Pollock, T. M.: A new tribeam system for three
361 dimensional multimodal materials analysis. *Rev Sci Instrum* 83:023701, 2012.
- 362 Gerstenberger, H, and Haase, G.: A highly effective emitter substance for mass spectrometric
363 Pb isotope ratio determinations, *Chem Geol*, 136:309–312, 1997.
- 364 Gradstein, F. M., Ogg, J. G., Smith, A. G., Bleeker, W., and Lourens, L.: A new geologic time
365 scale, with special reference to Precambrian and Neogene, *Episodes*, 27:83–100, 2004.



- 366 Heaman, L. M.: The application of U-Pb geochronology to mafic, ultramafic and alkaline
367 rocks: An evaluation of three mineral standards, *Chem Geol*, 261:42–51, doi:
368 10.1016/j.chemgeo.2008.10.021, 2009.
- 369 Heaney, P. J., Vicenzi, E. P., Giannuzzi, L. A., and Livi, K. J. T.: Focused ion beam milling:
370 A method of site-specific sample extraction for microanalysis of Earth and planetary
371 materials, *Am Mineral*, 86:1094–1099, 2001.
- 372 Herd, C. D. K., Moser, D. E., Tait, K. T., Darling, J. R., Shaulis, B. J., and McCoy, T. J.:
373 Crystallization of Baddeleyite in Basaltic Rocks from Mars, and Comparisons with the
374 Earth, Moon and Vesta, In: *Microstructural Geochronology: Planetary Records Down to*
375 *Atom Scale*, 137-166, 2018.
- 376 Ibanez-Mejia, M., Gehrels, G. E., Ruiz, J., Vervoort, J. D., Eddy, M. P., and Li, C.: Small-
377 volume baddeleyite (ZrO₂) U-Pb geochronology and Lu-Hf isotope geochemistry by LA-
378 ICP-MS. Techniques and applications, *Chem Geol*, 384:149–167, doi:
379 10.1016/j.chemgeo.2014.07.011, 2014.
- 380 Jaffey, A. H., Flynn, K. F., Glendenin, L. E., Bentley, W. C., and Essling, A. M.: Precision
381 measurement of half-lives and specific activities of ²³⁵U and ²³⁸U, *Phys Rev*, 4:1889–
382 1906, 1971.
- 383 Krogh, T. E.: Improved accuracy of U-Pb zircon ages by the creation of more concordant
384 systems using an air abrasion technique, *Geochim Cosmochim Acta*, 46:637–649, 1982.
- 385 Krogh, T. E.: A low contamination method for hydrothermal decomposition of zircon and
386 extraction of U and Pb for isotopic age determinations, *Geochim Cosmochim Acta*,
387 37:485–494, 1973.
- 388 Matsui, S., Kaito, T., Fujita, J. I., Komuro, M., Kanda, K., and Haruyama, Y.: Three-
389 dimensional nanostructure fabrication by focused-ion-beam chemical vapor deposition, *J*
390 *of Vac Sci Technol B Microelectron Nanom Struct Process Meas Phenom*, 18:3181–3184,
391 2000.
- 392 Moser, D. E., Chamberlain, K. R., Tait, K. T., Schmitt, A. K., Darling, J. R., Barker, I. R.,
393 Hyde, B. C.: Solving the Martian meteorite age conundrum using micro-baddeleyite and
394 launch-generated zircon, *Nature*, 499:454–7, doi: 10.1038/nature12341, 2013.
- 395 Moser, D. E., Cupelli, C. L., Barker, I. R., Flowers, R. M., Bowman, J. R., Wooden, J., and
396 Hart, J. R.: New zircon shock phenomena and their use for dating and reconstruction of
397 large impact structures revealed by electron nanobeam (EBSD, CL, EDS) and isotopic U-



- 398 Pb and (U-Th)/He analysis of the Vredefort dome, *Can J Earth Sci* 48:117–139, doi:
399 10.1139/E11-011, 2011.
- 400 Paquette, J-L., Goncalves, P., Devouard, B., Nicollet, C.: Micro-drilling ID-TIMS U-Pb dating
401 of single monazites: A new method to unravel complex poly-metamorphic evolutions.
402 Application to the UHT granulites of Andriamena (North-Central Madagascar), *Contrib*
403 *to Mineral Petrol*, 147:110-122, 2004.
- 404 Parrish, R. R., and Noble, S. R.: Zircon U-Th-Pb Geochronology by Isotope Dilution - Thermal
405 Ionization Mass Spectrometry (ID-TIMS). In: Hancher JM, Hoskin PWO (eds) *Reviews*
406 *in Mineralogy and Geochemistry: Zircon*. Mineralogical Society of America, Washington
407 DC, 183–213, 2003.
- 408 Pietrzak-Renaud, N., and Davis, D.: U-Pb geochronology of baddeleyite from the Belleview
409 metadiabase: Age and geotectonic implications for the Negaunee Iron Formation,
410 Michigan, *Precambrian Res*, 250:1–5, 2014.
- 411 Reddy, S. M., van Riessen, A., Saxey, D. W., Johnson, T. E., Rickard, W., Fougereuse, D.,
412 Fischer, S., Prosa, T. J., Rice, K. P., Reinhard, D. A., Chen, Y., and Olson, D.:
413 Mechanisms of deformation-induced trace element migration in zircon resolved by atom
414 probe and correlative microscopy, *Geochim Cosmochim Acta*, 195, 158–170, doi:
415 10.1016/j.gca.2016.09.019, 2016.
- 416 Reinhard, D. A., Moser, D. E., Martin, I., Rice, K. P., Chen, Y., Olson, D., Lawrence, D., Prosa,
417 T. J., and Larson, D. J.: Atom Probe Tomography of Phalaborwa Baddeleyite and
418 Reference Zircon BR266, In: *Microstructural Geochronology: Planetary Records Down*
419 *to Atom Scale*, 315–326, 2018.
- 420 Reischmann, T.: Precise U/Pb age determination with baddeleyite (ZrO₂), a case study from
421 the Phalaborwa igneous complex, South Africa, *South African J Geol*, 98:1–4, 1995.
- 422 Romer, R. L.: Alpha-recoil in U-Pb geochronology: Effective sample size matters, *Contrib to*
423 *Mineral Petrol*, 145:481–491, 2003.
- 424 Schaffer, M., Schaffer, B., and Ramasse, Q.: Sample preparation for atomic-resolution STEM
425 at low voltages by FIB, *Ultramicroscopy*, 114:62–71, 2012.
- 426 Schmitt, A. K., Chamberlain, K. R., Swapp, S. M., Harrison, T. M.: In situ U-Pb dating of
427 micro-baddeleyite by secondary ion mass spectrometry, *Chem Geol* 269:386–395, doi:
428 10.1016/j.chemgeo.2009.10.013, 2010.



- 429 Smith, N. S., Skoczylas, W. P., Kellogg, S. M., Kinion, D. E., and Tesch, P. P.: High brightness
430 inductively coupled plasma source for high current focused ion beam applications, *J*
431 *Vacuum Sci Technol B*, 24:2902–2906, 2006.
- 432 Soderlund, U., and Johansson, L.: A simple way to extract baddeleyite (ZrO₂), *Geochemistry*
433 *Geophys Geosystems*, 3:1014. doi: 10.1029/2001gc000212, 2002.
- 434 White, L. F., Darling, J. R., Moser, D. E., Reinhard, D. A., Dunlop, J., Larson, D. J., Lawrence,
435 D., and Martin, I.: Complex nanostructures in shocked, annealed and metamorphosed
436 baddeleyite defined by atom probe tomography, In: Moser D, Corfu F, Reddy S, et al.
437 (eds) *Microstructural Geochronology: Planetary Records Down to Atom Scale*, John
438 Wiley & Sons, Inc, Hoboken, NJ, 2017a.
- 439 White, L. F., Darling, J. R., Moser, D. E., Reinhard, D. A., Prosa, T. J., Bullen, D., Olson, D.,
440 Larson, D., and Martin, I.: Atomic scale age resolution of planetary events, *Nat Commun*.
441 doi: 10.1038/ncomms15597, 2017b.
- 442 Wingate, M. T. D., and Compston, W.: Crystal orientation effects during ion microprobe U –
443 Pb analysis of baddeleyite, *Chem Geol*, 168:75–97, 2000.
- 444 Yuan, X., Wehrs, J., Ma, H., Al-Samman, T., Korte-Kerzel, S., Goken, M., Michler, J.,
445 Spolenak, R., and Wheeler, J. M.: Investigation of the deformation behaviour of
446 aluminium micropillars produced by focused ion beam machining using Ga and Xe ions,
447 *Scr Mater* 127:191–194, 2017.
- 448 Ziegler, J. F., Biersack, J. P., and Littmark, U.: *The stopping range of ions in matter*. New York,
449 USA, 1985.
- 450
451
452
453
454
455
456
457
458
459
460
461
462



468
469
470
471
472
473
474
475
476
477
478
479
480
481
482
483
484
485
486
487
488
489
490
491
492
493
494
495
496
497
498
499

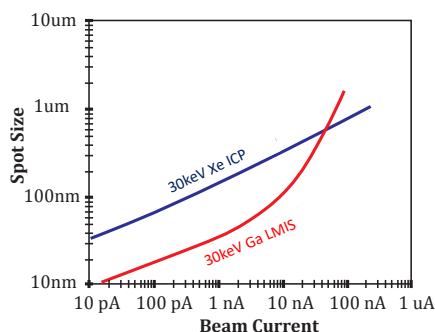
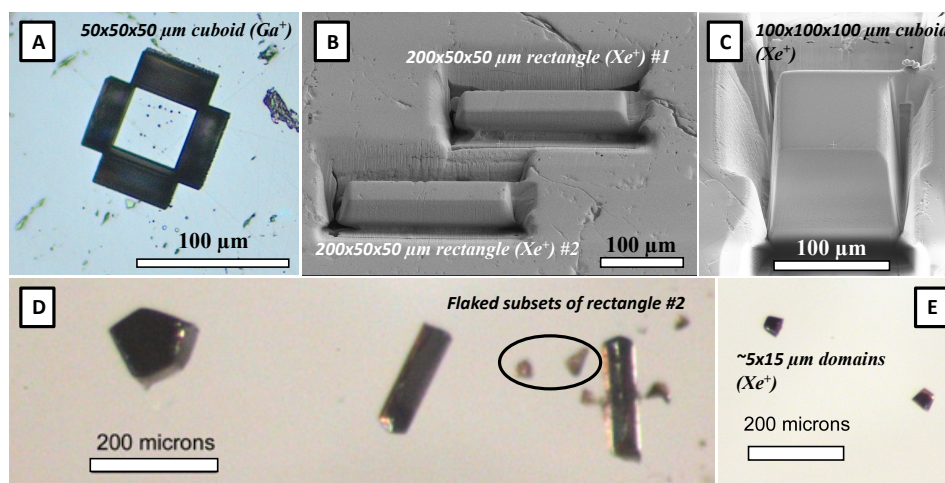
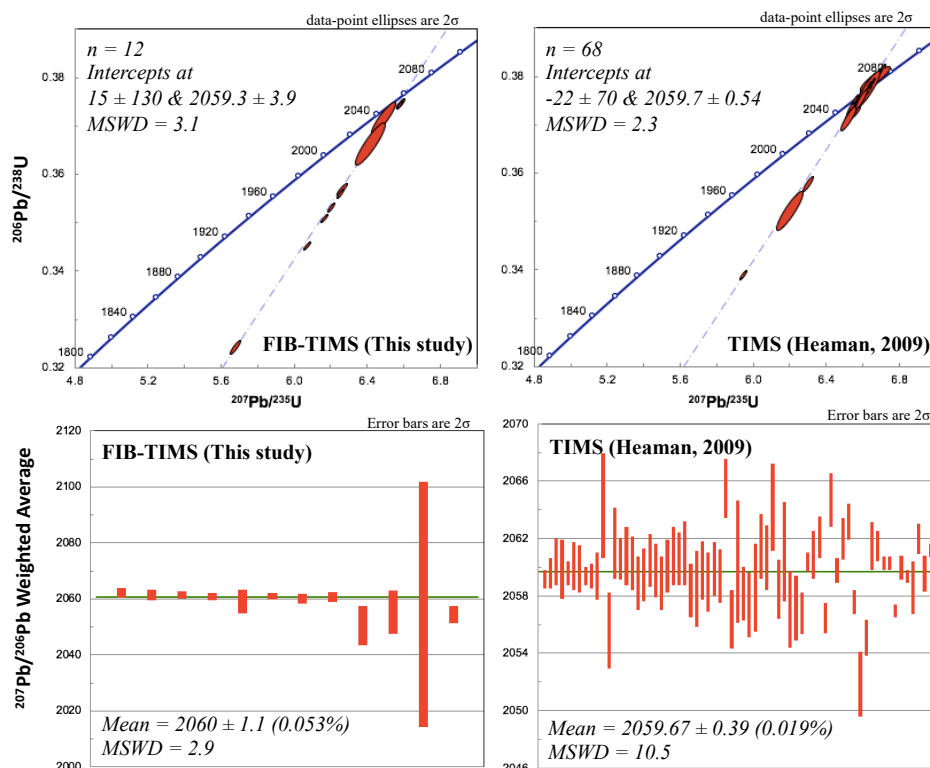


Figure 1: Spot size versus beam current for Xe^+ and Ga^+ source focused ion beam (FIB) instruments. At higher beam currents (> 10 nA) the spot size generated by the liquid metal ion source (LMIS) Ga^+ FIB exponentially increases due to spherical aberration, limiting the energy that can be applied during milling. The inductively coupled Xe pFIB source remains stable at higher currents, yielding a linear increase in spot size with beam current and allowing higher energies to be applied without sacrificing spatial precision. This opens the door to larger scale (millimetre) milling experiments, such as extracting whole mineral phases from thin section or grain mount. Adapted after (Burnett et al. 2016).



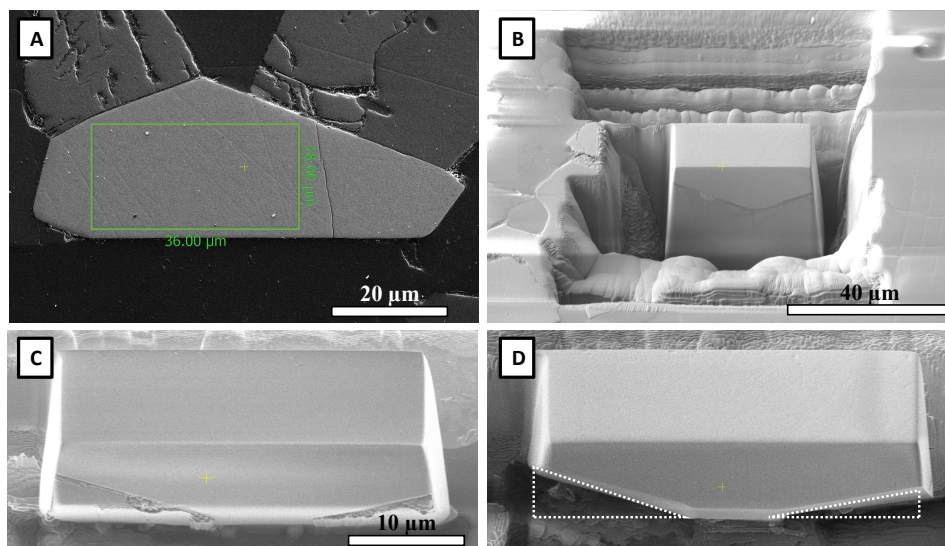
500 **Figure 2:** Optical microscopy and secondary electron (SE) imaging of isolated
501 baddeleyite domains in Phalaborwa baddeleyite mount. The small amount of material
502 left to anchor the domains (A - C) is critical in transporting the mount without losing
503 material, and in ensuring easy extraction without the need for tungsten weld or
504 complicated and time-consuming micro-manipulator usage. Once released from the
505 grain mount, samples can be broken into further sub samples (D) and extensively
506 images (E). All of the FIB extracted samples used for TIMS analyses, as denoted in
507 table 1, are imaged here.

508
509
510
511
512
513
514
515
516
517
518
519
520
521
522



523 **Figure 3:** U-Pb concordia diagrams and weighted average Pb-Pb ages for data
524 generated by FIB-TIMS and TIMS analysis of the Phalaborwa baddeleyite reference
525 material within this study (left). For comparison, all U-Pb and Pb-Pb data reported by
526 Heaman, 2009, are also presented (right), highlighting the natural discordance and
527 variation within the Phalaborwa baddeleyite population.

528
529
530
531
532
533
534
535
536
537
538



539 **Figure 4:** Xe^+ pFIB images detailing the extraction of a 36 x 18 μm domain of a large (50
540 μm) baddeleyite grain from a thin section of the Duluth gabbro (A). During large scale
541 cutting (B), small domains of common-Pb bearing feldspar remained attached to the target
542 baddeleyite (C), though these were quickly removed using the Xe^+ pFIB instrument through a
543 series of tilted and rotated cuts to produce a single grain with no rim or inclusions (D).

544
545
546
547
548
549
550
551
552
553
554
555
556
557
558
559



	U (ppm)	Total Pb (pg)	Common Pb (pg)	206Pb/238 Age (Ma)	$\pm 2\sigma$	207Pb/235U Age (Ma)	$\pm 2\sigma$	207Pb/206 Age (Ma)	$\pm 2\sigma$	% Disc
No FIB Exposure										
1 chip from mount	3027	1321	12.29	1912	3	1985	2	2062	2	8.4
5 chips from mount	1591	464	1.09	2052	4	2057	2	2062	2	0.6
Whole grain #1	431	94	0.17	2052	4	2057	2	2061	1	0.5
Whole grain #2	277	151	0.18	2051	3	2056	2	2061	1	0.6
Ga-FIB										
50x50x50 um cube	443	62	1.91	1968	4	2013	3	2059	4	5.1
Xe-FIB										
100x100x100 um cube	397	757	0.54	1950	3	2005	2	2061	1	6.2
200x50x50 um rectangle #1	284	246	0.66	1964	4	2011	2	2060	2	5.4
200x50x50 um rectangle #2	352	301	1.28	1940	3	1999	2	2061	2	6.8
Flake (subset of rectangle #2)	106	6	0.33	2038	13	2044	7	2051	7	0.7
Flake (subset of rectangle #2)	254	5	0.67	2013	17	2034	9	2055	8	2.4
5x15um domain #1	508	16	6.24	1995	9	2026	26	2058	44	3.6
5x15um domain #2	510	13	0.25	1811	6	1927	3	2055	3	13.6

550
 551 **Table 1:** U-Pb age data generated by TIMS and FIB-TIMS analyses of the Phalaborwa
 552 baddeleyite reference material. Further details, including raw U/Pb counts and ratios, can be
 553 found in the supplementary materials.